Shape Deformation in Two-Dimensional Electrical Impedance Tomography

Alistair Boyle, Andy Adler and William R. B. Lionheart

Abstract—Electrical Impedance Tomography (EIT) uses measurements from surface electrodes to reconstruct an image of the conductivity of the contained medium. However, changes in measurements result from both changes in internal conductivity and changes in the shape of the medium relative to the electrode positions. Failure to account for shape changes results in a conductivity image with significant artifacts. Previous work to address shape changes in EIT has shown that in some cases boundary shape and electrode location can be uniquely determined for isotropic conductivities; however, for geometrically conformal changes, this is not possible. This prior work has shown that the shape change problem can be partially addressed. In this paper, we explore the limits of compensation for boundary movement in EIT using three approaches: first, a theoretical model was developed to separate a deformation vector field into conformal and non-conformal components, from which the reconstruction limits may be determined; next, finite element models were used to simulate EIT measurements from a domain whose boundary has been deformed; finally, an experimental phantom was constructed from which boundary deformation measurements were acquired. Results, both in simulation and with experimental data, suggest that some electrode movement and boundary distortions can be reconstructed based on conductivity changes alone while reducing image artifacts in the process.

I. Introduction

ELECTRICAL Impedance Tomography (EIT) applies current and measures voltage through electrodes on the surface to reconstruct a conductivity distribution for the interior of the domain. In medical EIT, errors in knowledge of the boundary shape are an important factor in the accuracy of reconstructions. This is a significant factor for chest EIT where the chest shape deforms as the patient breathes and changes posture [1], [2].

In general terms, if a distortion is applied to a domain in two- or three-dimensional space, the assumed isotropy (uniformity in all directions) of the conductivity distribution is not preserved [3]. If the conductivity is assumed to be isotropic, the boundary voltage and current data on the distorted domain will generally not be consistent with an isotropic conductivity. This means that in the isotropic case, the set of boundary data contains information about both the conductivity and the boundary shape.

While all distortions are equivalent to a generalized (possibly anisotropic) conductivity change on a domain with the original shape, a subset of these distortions can be modelled as isotropic conductivity changes with the original shape. This subset is exactly the distortions that are conformal maps. In two-dimensional space, there is an infinite-dimensional space of conformal maps, whereas in three dimensions, there is a finite-dimensional space of conformal maps, the Möbius transformations [4].

In many industrial applications where the dimensions of the boundary are fixed, such as mixing vessels [5], accurately acquiring the boundary information is practical through careful measurements. In practise, we would not usually want to use electrical measurements to recover the boundary shape, as one could employ mechanical or optical measurement devices to determine the external shape of the body and the position of the electrodes [6], [7]. As previously noted, in many biomedical settings and particularly in the case of lung imaging, this boundary is continuously changing [1], [2]. Lung imaging is an important application of EIT because it offers the opportunity to provide continuous monitoring of patients placed on ventilation support [8]. In this application, electrodes are attached about the circumference of the chest. The boundary shape of the chest changes with breathing, so it is desirable to correct the unknown boundary shape using the EIT data so that a consistent isotropic conductivity can be fitted to the data. To achieve this, Soleimani *et al.* suggested a method where the electrode positions are perturbed in an attempt to better fit the measurement data to the reconstruction for small changes in the boundary [9]. This technique should result in a distorted image due to the anisotropic nature of chest muscle, yet still preserve useful features of the lungs.

This type of shape correction could also be interpreted as a type of model reduction error, using the framework developed by Kolehmainen *et al.* to address inexact knowledge of the boundary shape [10], [11]. The relationship between an exact and geometrically inexact domain is modelled [10], [12] (which was extended to contact impedance errors [13]) and once first- and second-order statistics are computed, combined into the inverse formulation. This results in the addition of a dense model error matrix to the reconstruction error term. The approach of Soleimani *et al.* gives a formulation that is structurally similar to the model reduction approach of Kolehmainen *et al.* but is motivated by considering the ability to reconstruct additional features from the data.

In this paper, we explore the ability and limits of EIT to resolve conductivity changes and reject boundary distortion. First, we show that the particular behaviour of conformal deformations in EIT given in previous theoretical work [3] still holds in the case of a finite number of electrodes and a finite element discretization of the forward problem. Our

A. Boyle and A. Adler are with the Department of Systems and Computer Engineering, Carleton University, Ottawa, ON e-mail: boyle@sce.carleton.ca

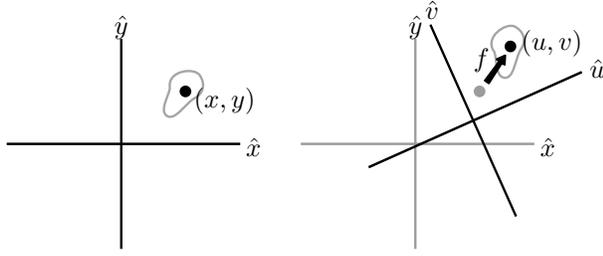William R. B. Lionheart is with the University of Manchester.

Fig. 1: A change of coordinate systems transforms the point (x, y) to the new coordinates (u, v); the old coordinates (x, y) relative to the original x-, y-axes are at the same location as the new coordinates relative to the new axes where in this case, a translation and rotation have been applied. The transformation need not lead to a rectilinear coordinate system.

example simulations in two dimensions, using a linearization of the forward problem, suggest that the boundary shape and electrode positions can be recovered up to an infinitesimal conformal map. This provides an adequate and necessary correction for acceptable reconstruction of the conductivity. We also observe the effect of the size of the electrodes and note that the area (or length in two dimensions) of the electrodes is not preserved by conformal mappings [14]. In addition, we observe that conformal deformations modelled by translating nodes on a Finite Element Method (FEM) mesh with a piecewise linear discretization of the domain, fail to locally preserve angles in the mesh. These changes in angle introduce voltage changes at interior mesh nodes where none would be otherwise expected. In order to validate these results experimentally, we develop a deformable phantom from which we test the theoretical and simulated results.

II. FINITE ELEMENT DEFORMATIONS

We are motivated by the question: when a boundary deformation occurs, is it possible for the conductivity to change to allow the voltages over the domain to remain the same? The result is well known amongst mathematicians, but we here include an explanation we hope will be easily accessible to the broader impedance imaging community.

To explore this question, the weak form of EIT's constitutive equation is examined as it is applied in the EIT FEM model:

$$\int_\Omega w\nabla \cdot \sigma\nabla\phi \, \mathrm{d}V = 0 \qquad (1)$$

where w is a test function selected to achieve a minimal residual, σ is a tensor conductivity (isotropic or anisotropic) and ϕ is potential throughout the domain Ω. In two dimensions, a deformation is defined by some coordinate transformation from (x, y) to (u, v) coordinates:

$$(u, v) = f(x, y) \qquad (2)$$

This can be thought of as a transformation of the coordinate system from a Euclidean (x, y) to (u, v) in a new coordinate system (Figure 1). When a deformation occurs, it results in a new conductivity σ' and potential distribution ϕ' over the

domain as well as some change in the volume $\mathrm{d}V'$ over which the integral is calculated. A new test function w' is also introduced.

$$\int_\Omega w\nabla \cdot \sigma\nabla\phi \, \mathrm{d}V = \int_{\Omega'} w'\nabla \cdot \sigma'\nabla\phi' \, \mathrm{d}V' \qquad (3)$$

A linear transformation can be represented by a set of partial derivatives of the transformation function

$$\begin{bmatrix} \frac{\partial}{\partial x} \\ \frac{\partial}{\partial y} \end{bmatrix} = \begin{bmatrix} a & b \\ c & d \end{bmatrix} \begin{bmatrix} \frac{\partial}{\partial u} \\ \frac{\partial}{\partial v} \end{bmatrix} \qquad (4)$$

where $a = \frac{\partial u}{\partial x}$, $b = \frac{\partial v}{\partial x}$, $c = \frac{\partial u}{\partial y}$, and $d = \frac{\partial v}{\partial y}$. The inverse of the transformation gives

$$\begin{bmatrix} \frac{\partial}{\partial u} \\ \frac{\partial}{\partial v} \end{bmatrix} = \underbrace{\frac{1}{ad - bc}\begin{bmatrix} d & -b \\ -c & a \end{bmatrix}}_{\mathbf{T}} \begin{bmatrix} \frac{\partial}{\partial x} \\ \frac{\partial}{\partial y} \end{bmatrix} \qquad (5)$$

where $\mathbf{T}$ is the two-by-two inverse of the transformation matrix (4). The volume derivative of the transformation scales by the determinant.

$$\mathrm{d}V' = \frac{1}{\det(\mathbf{T})}\,\mathrm{d}V \qquad (6)$$

Using (3), the new conductivity σ' must be modified in some way if the voltages throughout the domain are to be equal ($\phi = \phi'$). The test functions can be chosen arbitrarily and are set equal ($w = w'$). Expanding (3) into a matrix of partial derivatives gives

$$\begin{bmatrix} \frac{\partial}{\partial x} & \frac{\partial}{\partial y} \end{bmatrix} \sigma \begin{bmatrix} \frac{\partial}{\partial x} \\ \frac{\partial}{\partial y} \end{bmatrix} \phi \, \mathrm{d}V =$$
$$\begin{bmatrix} \frac{\partial}{\partial u} & \frac{\partial}{\partial v} \end{bmatrix} \sigma' \begin{bmatrix} \frac{\partial}{\partial u} \\ \frac{\partial}{\partial v} \end{bmatrix} \phi' \, \mathrm{d}V' \qquad (7)$$

where potential is equal ($\phi = \phi'$), though in different locations due to the transformation. This implies that the boundary data $\phi_{\partial\Omega}$ are the same, though the boundary measurement locations may differ, because the energy integrals (3) are equal. Using the chain rule with (5) (6) into (7) gives

$$\begin{bmatrix} \frac{\partial}{\partial x} & \frac{\partial}{\partial y} \end{bmatrix} \sigma \begin{bmatrix} \frac{\partial}{\partial x} \\ \frac{\partial}{\partial y} \end{bmatrix} \phi \, \mathrm{d}V =$$
$$\begin{bmatrix} \frac{\partial}{\partial x} & \frac{\partial}{\partial y} \end{bmatrix} \mathbf{T}^{\mathsf{T}}\sigma'\mathbf{T} \begin{bmatrix} \frac{\partial}{\partial x} \\ \frac{\partial}{\partial y} \end{bmatrix} \phi \frac{1}{\det(\mathbf{T})} \, \mathrm{d}V \qquad (8)$$

Simplifying (8) leaves

$$\sigma = \mathbf{T}^{\mathsf{T}}\sigma'\mathbf{T}\frac{1}{\det(\mathbf{T})} \qquad (9)$$

and rearranging for the new conductivity σ', gives

$$\sigma' = \mathbf{T}^{-\mathsf{T}}\sigma\mathbf{T}^{-1}\det(\mathbf{T}) \qquad (10)$$

which is a result (the push forward of the diffeomorphism) attributed by Kohn to Luc Tatar: a distortion that fixes points on the boundary leaves the Dirichlet-to-Neumann map invariant [15], [16].

Therefore, for an arbitrary conductivity tensor σ, for any transformation $\mathbf{T}$, the conductivity can be adjusted in some manner such that the new boundary data will match the old.

Fig. 2: Electrode current density under deformation
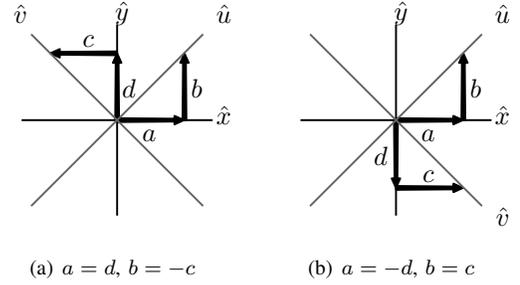

(a) $a = d$, $b = -c$ (b) $a = -d$, $b = c$

Fig. 3: The two conformal solutions; (a) and (b) are solutions for conformal transformations that will maintain an isotropic conductivity. Note that (b) is a solution that flips the $\hat{u}$-axis.

However, this equation provides no guarantee that an initially isotropic conductivity will map to a new conductivity that is also isotropic.

In a practical EIT system, the boundary voltage and currents are measured through electrodes. When the boundary deforms, these electrodes may deform to match the boundary or change shape depending on their mechanical properties. If the total current I_n through an electrode does not change, the current density J_n must change when a deformation changes the surface area of the electrode. In two dimensions, intuitively, the current density for an electrode must scale with the change in the length of the boundary associated with the electrode $1/\ell$. For a single electrode n,

$$I_n = \int J_n \, \mathrm{d}S = \int J'_n \, \mathrm{d}S' \tag{11}$$

$$J'_n = J_n \frac{\mathrm{d}S}{\mathrm{d}S'} \tag{12}$$

This observation clarifies one source of the artifacts observed due to movement of the boundary [14].

If the measurements ϕ remain constant when a deformation occurs and the initial conductivity is isotropic, when is the new conductivity σ' isotropic? Taking the conductivity equivalence (10) and assuming isotropic conductivity σ' gives

$$\sigma = \sigma' \mathbf{T}^{-\mathsf{T}} \mathbf{T}^{-1} \det(\mathbf{T}) \tag{13}$$

If conductivities, both before and after, are isotropic then

$$\mathbf{T}^{-\mathsf{T}} \mathbf{T}^{-1} \det(\mathbf{T}) = k\mathbf{I} \tag{14}$$

Expanding and then simplifying the equation

$$\frac{1}{ad - bc} \begin{bmatrix} a^2 + c^2 & ab + cd \\ ab + cd & b^2 + d^2 \end{bmatrix} = k\mathbf{I} \tag{15}$$

shows that $ab + cd = 0, a^2 + c^2 = b^2 + d^2$ and therefore $a = \pm d$, $c = \mp b$, hence $k = 1$.

The first solution $a = +d$ and $c = -b$ turns out to be the Cauchy-Riemann equations,

$$\frac{\partial u}{\partial x} - \frac{\partial v}{\partial y} = 0 \tag{16a}$$

$$\frac{\partial u}{\partial y} + \frac{\partial v}{\partial x} = 0 \tag{16b}$$

which shows that conformal deformations, and only conformal deformations, can result in a new isotropic conductivity if the original conductivity was isotropic. The alternative solution $a = -d$ and $c = +b$ corresponds to switching from a right-hand rule coordinate system to a left-hand rule coordinate system (Figure 3).
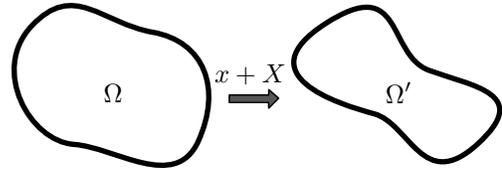

Fig. 4: A mapping of the domain Ω to Ω' by the vector field X

For an initially isotropic domain to remain isotropic after a deformation, that deformation must be conformal. To see why only a conformal deformation is acceptable, we examine the situation for an "infinitesimal" deformation X which maps $x \mapsto x + X$. (Figure 4). A *conformal map* is one that preserves the angles but not necessarily the lengths between vectors on the domain (Figure 5). An *infinitesimal* conformal map (*infinitesimal conformal motion*, *conformal Killing field* or more simply a *conformal vector field*) represents a small distortion that may be represented as a vector field X [17].

If the distorted domain is to have an isotropic field (e.g. conductivity in EIT) consistent with the boundary conditions, for a small change in the boundary of the domain Ω, the vector field X must be conformal and sufficiently smooth. Therefore, X must satisfy the conformal Killing field equation (i.e. the symmetrized derivative of X is a multiple of the identity) (17). [18, §3.7] [19, §1.3]

$$\frac{\partial X_i}{\partial x_j} + \frac{\partial X_j}{\partial x_i} = \alpha \delta_{ij} \tag{17}$$

where α is a scalar on the domain Ω [18, (3.7.3)] and shows how a change in dimension i is related to a change in dimension j.

If two tensors are equal, their traces are equal. In two dimensions, summing over i and j, α must be the divergence
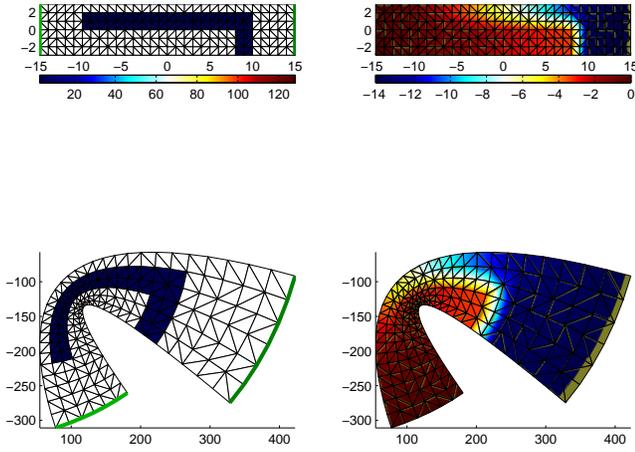
Fig. 5: A conformal mapping of a rectangular grid with the conformal map $z \to \exp((z - 20 - \mathrm{i}80)/100) \cdot (z + \mathrm{i}20) \cdot (z - \mathrm{i}10)$, top – rectangular region with electrodes across the ends and L-shaped inhomogeneity, bottom – conformal deformation applied to FEM mesh prior to simulation, left – FEM mesh and inhomogeneity, right – simulated voltage distributions. Lines still intersect at 90° after deformation. Voltages at individual nodes remain the same despite the deformation.

of X.

$$\mathrm{tr} \begin{bmatrix} \frac{\partial X_1}{\partial x_1} + \frac{\partial X_1}{\partial x_1} & \frac{\partial X_1}{\partial x_2} + \frac{\partial X_2}{\partial x_1} \\ \frac{\partial X_2}{\partial x_1} + \frac{\partial X_1}{\partial x_2} & \frac{\partial X_2}{\partial x_2} + \frac{\partial X_2}{\partial x_2} \end{bmatrix} = \mathrm{tr} \begin{bmatrix} \alpha & 0 \\ 0 & \alpha \end{bmatrix} \quad (18)$$

$$\alpha = \frac{\partial X_1}{\partial x_1} + \frac{\partial X_2}{\partial x_2} = \nabla \cdot X \quad (19)$$

Setting $i = j = 1$ or 2 gives the first Cauchy-Riemann equation,

$$2\frac{\partial X_1}{\partial x_1} = \frac{\partial X_1}{\partial x_1} + \frac{\partial X_2}{\partial x_2}$$

$$\frac{\partial X_1}{\partial x_1} - \frac{\partial X_2}{\partial x_2} = 0 \quad (20a)$$

and setting $i = 1, j = 2$ or $i = 2, j = 1$ gives the second Cauchy-Riemann equation,

$$\frac{\partial X_1}{\partial x_2} + \frac{\partial X_2}{\partial x_1} = 0 \quad (20b)$$

Thus, if a function X is differentiable, 1) its derivative is continuous and it satisfies the Cauchy-Riemann equations, and 2) it is complex analytic on the part of the plane that satisfies the Cauchy-Riemann equations. With any complex analytic function, the real and imaginary parts are harmonic conjugate [20]. Specifically, the components of a conformal vector field interpreted as a complex function $X_1 + \mathrm{i}X_2$ are complex analytic and satisfy $\nabla X_1 \cdot \nabla X_2 = 0$, $|\nabla X_1|^2 = |\nabla X_2|^2$, and Laplace's equation $\nabla^2 X_1 = \nabla^2 X_2 = 0$. The components of the vector field (X_1, X_2) are perpendicular, but furthermore, ∇X_2 is 90° anti-clockwise from ∇X_1 and equal in magnitude (Figure 6).

This relationship matches our previously derived relationship (16a) (16b) for a two-dimensional deformation where the conductivity remains isotropic throughout. This can be seen

Fig. 6: Derivatives of the components of a conformal vector field at the boundary

by performing a change of variables on (16a) (16b) so that we are instead operating on an "infinitesimal" deformation $x \mapsto x + X$ in two dimensions. Using $x \to x_1$, $y \to x_2$, so that $u \to x_1 + X_1$, $v \to x_2 + X_2$, then

$$\frac{\partial u}{\partial x} - \frac{\partial v}{\partial y} = 0$$

$$1 + \frac{\partial X_1}{\partial x_1} - 1 - \frac{\partial X_2}{\partial x_2} = 0 \quad (21)$$

Thus, (20a) matches (16a),

$$\frac{\partial u}{\partial y} + \frac{\partial v}{\partial x} = 0$$

$$0 + \frac{\partial X_1}{\partial x_2} + 0 + \frac{\partial X_2}{\partial x_1} = 0 \quad (22)$$

and (20b) matches (16b) as well. This shows the correspondence between our initial FEM-based description and the vector field based derivation but also illustrates why there are many conformal deformations possible in two dimensions: the initial conditions of the deformation cancel (21) (22) while in higher dimensions this may not be the case.

Using the Cauchy-Riemann equations (20a) (20b) and the Dirichlet-to-Neumann map Λ_σ, a further observation for a known conductivity distribution can be drawn: knowing one portion of a conformal deformation on the boundary X_1 dictates the other X_2. Recall the conductivity equation $\nabla \cdot \sigma \nabla \phi = 0$ and that a Dirichlet-to-Neumann map Λ_σ takes a potential ϕ restricted to the boundary of the domain $\partial \Omega$ and maps it to a current density $J = \sigma \partial \phi / \partial \hat{n}$ where $\hat{n}$ is the outward unit normal on the boundary. In particular, the Dirichlet-to-Neumann map Λ_1 is a solution for Laplace's equation with conductivity $\sigma = 1$. In EIT, this map $\Lambda_1 : \phi|_{\partial \Omega} \mapsto J$ is solved using an FEM over any arbitrarily shaped domain. This same map can be used to solve Laplace's equation such that $\Lambda_1 : \phi|_{\partial \Omega} \mapsto X$, where the operator Λ_1 is no longer acting as a transconductance operator but instead as a voltage-to-movement operator.

The Dirichlet-to-Neumann operator Λ_1 is used to convert Dirichlet data on the boundary $X_1|_{\partial \Omega}$ to Neumann data normal to the boundary ($\nabla X_1 \cdot \hat{n}$) which is the same as the tangential Neumann boundary data for X_2 ($\nabla X_2 \cdot \hat{t}$).

$$\Lambda_1 \phi \Big|_{\partial \Omega} = \nabla \phi \cdot \hat{n} = \frac{J_n}{\sigma} \quad (23)$$

$$\Lambda_1 X_1 \Big|_{\partial \Omega} = \nabla X_1 \cdot \hat{n} = \nabla X_2 \cdot \hat{t} \quad (24)$$

where $\hat{t}$ is the tangent vector and $\hat{n}$ is the normal vector on the boundary $\partial \Omega$.

Knowing the tangential derivative of X_2 at the boundary

is essentially the same as knowing the Dirichlet data for X_2 since it can be integrated along the boundary.

$$\nabla X_2 \cdot \hat{t} = \frac{\partial X_2}{\partial s} \qquad (25)$$

where s is the anti-clockwise arc length along the boundary $\partial \Omega$.

Combining (24) (25) and integrating along $\mathrm{d}s$ gives

$$X_2 = \int_0^s \Lambda_1 X_1 \, \mathrm{d}s + \text{const} \qquad (26)$$

such that X_1 and X_2, within the domain Ω, are determined by values on the boundary $\partial \Omega$, and the boundary values of a conformal X are exactly those with

$$X_2 - \int_0^s \Lambda_1 X_1 \, \mathrm{d}s = \text{const} \qquad (27)$$

or

$$\frac{\partial}{\partial s} X_2 - \Lambda_1 X_1 = 0 \qquad (28)$$

and in matrix form

$$\begin{bmatrix} -\Lambda_1 & L_1 \end{bmatrix} \begin{bmatrix} X_1 \\ X_2 \end{bmatrix} = 0 \qquad (29)$$

where L_1 is the difference operator along the boundary $\frac{\partial}{\partial s}$.

Thus, X_1 can be specified arbitrarily on the boundary, and its tangential derivative $\mathrm{d}X_2/\mathrm{d}s$ is determined. X_2 is the solution of a Neumann problem for Laplace's equation and is determined up to a constant. Constants added to X_1 and X_2 correspond to a translation which would not be expected in EIT data.

This means that, in the discrete setting of the FEM, specifying a distortion on the boundary nodes will give a unique conformal map. In the FEM setting, the infinitesimal vector field X becomes a vector that translates each node of the finite element mesh. Simply applying the vector field to the mesh will result in a globally conformal transformation, but locally about the nodes, the angles between edges joining elements will have changed. The vector field X is continuous, and therefore, an accurate application of the field will "bend" the shape of the mesh elements to maintain the local angles about each node.

Applying this new knowledge to an EIT problem using the FEM, we can expect that an approximately conformal discrete deformation of a body with an isotropic conductivity will result in the same measurements at the boundary. Conversely, other deformations that exclude conformal changes will result in different measurements at the boundary unless the conductivity is changed to some specific anisotropic distribution.

III. SIMULATED CONFORMAL MOTION

In the previous section, we explored the analytic solution for complete boundary data. In EIT, we have discrete electrodes and so must deal with incomplete boundary data that does not exactly match the analytic solution. Our example simulations using a two-dimensional linearization of the forward problem (simulations in EIDORS [21]) suggest that the boundary shape and electrode positions can be recovered up to an infinitesimal

conformal map. This testing shows that despite conformal effects, boundary shape correction provides an adequate and necessary correction for acceptable reconstruction of the conductivity.

To test the behaviour of an isotropic conductivity when a conformal deformation was applied, a convergence study was undertaken where a conformal deformation was selected and the difference between the undeformed and deformed simulations was observed to converge as the number of nodes in the FEM model was increased. The undeformed simulation consisted of a rectangular domain with an electrode extending across either end. An L-shaped non-conductive region was set in the middle between the two electrodes (conductivity $\sigma = 0.01$ S/m, background 1 S/m). To exactly control the boundary conditions, a Complete Electrode Model (CEM) for each of the two electrodes was approximated using Point Electrode Models (PEMs) at individual nodes and current was distributed across these to achieve the appropriate current density boundary condition. When the deformation was applied, the current density was adjusted by the deformation, and no further manipulation of the PEM currents was required.

At each step, the forward simulation of the conductivity distribution shown in Figure 7(a) was computed to find the voltage on the domain at the nodes. The voltage at the FEM nodes was compared to the voltage after the FEM nodes were conformally deformed. As an example, the following conformal deformation was selected for these simulations:

$$z \to \frac{z - 20 + 80\mathrm{i}}{100}(z + 20i)(z - 10i), \qquad z = x + y\mathrm{i} \quad (30)$$

(shown in Figure 7(b)).

The number of nodes in the simulations ranged from 217 nodes to 455,000 nodes. Throughout this range, the triangular elements remained approximately equilateral. Convergence was measured as the 2-norm of the difference between the original voltages and the voltages on the mesh after the conformal deformation was applied and normalized against the average of the original voltages ($||V_2 - V_1||/||V_1||$). As the number of nodes increased and consequently, the element size was reduced towards a differential approximation, convergence of the undeformed and deformed voltages was observed. (Figure 7(c))

In order to explore the effect of reconstructing EIT images from media with conformal and non-conformal conductivity changes, two-dimensional simulations were constructed. Measurements were simulated for two distortion fields using a 576 element unit circular FEM mesh with adjacent stimulation and measurement on 16 point electrodes. Representing each boundary point by a complex $z = x + iy$, the distortions were

$$z \to 0.99x + \mathrm{i}1.01y \qquad \textit{Non-conformal} \qquad (31)$$
$$z \to z + 0.01z^2 \qquad \textit{Conformal} \qquad (32)$$

Additionally, one small conductive target and one small non-conductive target were simulated.

The conductivity images were reconstructed in a typical manner for EIT using a Tikhonov regularized single-step Gauss-Newton solver appropriate for small conductivity

(a) ORIGINAL
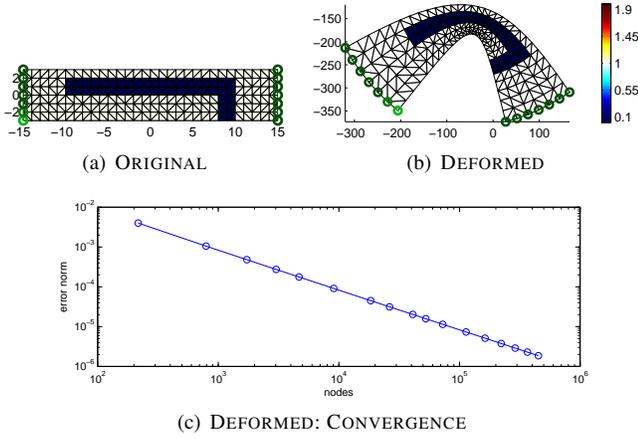
(b) DEFORMED

(c) DEFORMED: CONVERGENCE

Fig. 7: Conformal deformation convergence; (a) the original problem, (b) the conformal deformation (c) plots of the error norm between the deformed and undeformed voltage distributions; (c) shows solution convergence for (b) as the number of nodes in the FEM mesh increases

changes

$$\hat{\mathbf{x}}_0 = (\mathbf{J}_0^\mathsf{T}\mathbf{J}_0 + \lambda\mathbf{L}_0)^{-1}\mathbf{J}_0^\mathsf{T}\mathbf{y} = \mathbf{R}_0\mathbf{y} \qquad (33)$$

where $[\mathbf{y}]_i = [\mathbf{v}_{t2}]_i/[\mathbf{v}_{t1}]_i - 1$ is the normalized difference between boundary voltage measurements at an initial time $\mathbf{v}_{t1}$ and a later time $\mathbf{v}_{t2}$ due to a set of stimulation currents. The Jacobian $\mathbf{J}_0$ was calculated as the sensitivity of the measurements $\mathbf{y}$ to perturbations of the conductivity given an initial homogeneous conductivity $\mathbf{x}_1$.

$$\mathbf{J}_0 = \left.\frac{\partial\mathbf{y}}{\partial\mathbf{x}}\right|_{\mathbf{x}_1} \qquad (34)$$

A regularization matrix $\mathbf{L}_0$ was formed from an estimate of the image covariance [22]. The Tikhonov factor λ was selected heuristically as a compromise between noise and image resolution.

In the time interval between when the two measurements $\mathbf{v}_{t1}$ and $\mathbf{v}_{t2}$ are acquired, both the boundary shape and the conductivity of the interior may have changed. This can occur when a subject is breathing during lung EIT measurements. To account for this, the method of Soleimani *et al.* was adopted [9]. This uses the same reconstruction technique of (33) but adds to the equations to account for small movements of the electrodes. The reconstruction becomes

$$\hat{\mathbf{x}}_m = (\mathbf{J}_m^\mathsf{T}\mathbf{J}_m + \lambda\mathbf{L}_m)^{-1}\mathbf{J}_m^\mathsf{T}\mathbf{y} = \mathbf{R}_m\mathbf{y} \qquad (35)$$

where the Jacobian matrix $\mathbf{J}_m$, regularization matrix $\mathbf{L}_m$ and the resulting solution $\hat{\mathbf{x}}_m$ contain additional components related to the electrode movement. The Jacobian is augmented with a model of the data variance due to electrode movement calculated as a Jacobian due to linear electrode displacements using the approach of Soleimani *et al.* [9] where

$$\mathbf{J}_m = \begin{bmatrix} \mathbf{J}_0 & 0 \\ 0 & \mathbf{J}_e \end{bmatrix} \quad ; \quad \mathbf{J}_e = \left.\frac{\partial\mathbf{y}}{\partial\mathbf{m}}\right|_{\mathbf{x}_1} \qquad (36)$$

where $\mathbf{J}_e$ is the change in measurements $\mathbf{y}$ due to small

changes in electrode location $\mathbf{m}$ given an initial homogeneous conductivity $\mathbf{x}_1$. The new components of the Jacobian can be calculated through perturbing each electrode in the x and y directions. A more efficent algorithm is presented by Gómez-Laberge *et al.* [23]. Similarly, regularization was applied to the new electrode movement component of the Jacobian so that

$$\mathbf{L}_m = \begin{bmatrix} \mathbf{L}_0 & 0 \\ 0 & \frac{\mu}{\lambda}\mathbf{L}_e \end{bmatrix} \qquad (37)$$

$$\mathbf{L}_{e(i,j)} = \begin{cases} 2.1 & \text{if } i = j \\ -1 & \text{for adjacent electrodes} \\ 0 & \text{otherwise} \end{cases} \qquad (38)$$

The values of the regularization matrix were selected by Soleimani *et al.* to model the correlation between adjacent electrodes and ignores the correlation between all other electrodes. The value 2.1 was used to impose a penalty on global movement. The new regularization parameter μ was used to adjust the relationship between the conductivity and movement regularization. The new parameter is required because the two components of the regularization matrix are in different units. The parameter does have a practical relationship between the magnitude of expected conductivity changes and electrode movement, but in this case, the value was selected heuristically to minimize noise at the boundary while maintaining reasonably minimal electrode movement.

The results are shown in Figure 8. For the case of non-conformal movements, there are dramatic artifacts in the conductivity only reconstruction, and there is a clear benefit to movement reconstruction. In the case of conformal movements, no such benefit is seen, and the movement reconstruction is unable to detect movement. Combined conformal and non-conformal deformation showed only the non-conformal components of the deformation in the reconstructions.

IV. PHANTOM

Having shown that the movement compensation algorithm of Soleimani *et al.* [9] reduces artifacts for non-conformal deformations in simulation, while not being significantly affected by conformal deformations, experiments using a phantom were designed to test whether it is possible to reconstruct the conformal component of a deformation and that artifacts are indeed reduced by employing movement compensation. A deformable phantom was developed and used to obtain *in vitro* EIT measurements.

The phantom was constructed of a sponge rubber plumbing gasket placed in a shallow pan. The gasket formed a thick rubber ring that was easily compressed yet rigid enough to return to its original shape. Sixteen electrodes were constructed from stainless-steel wire pressed into the gasket and then looped over the edge of the gasket such that they lay along the inner wall of the gasket in a vertical orientation. An additional stainless-steel electrode placed roughly in the geometric centre of the gasket formed the ground connection. A shallow layer of saline solution was employed to limit conductivity in the vertical direction which presented an approximately two-dimensional section for the experimental measurements. The electrodes were each wired to a terminal bolted to the plastic
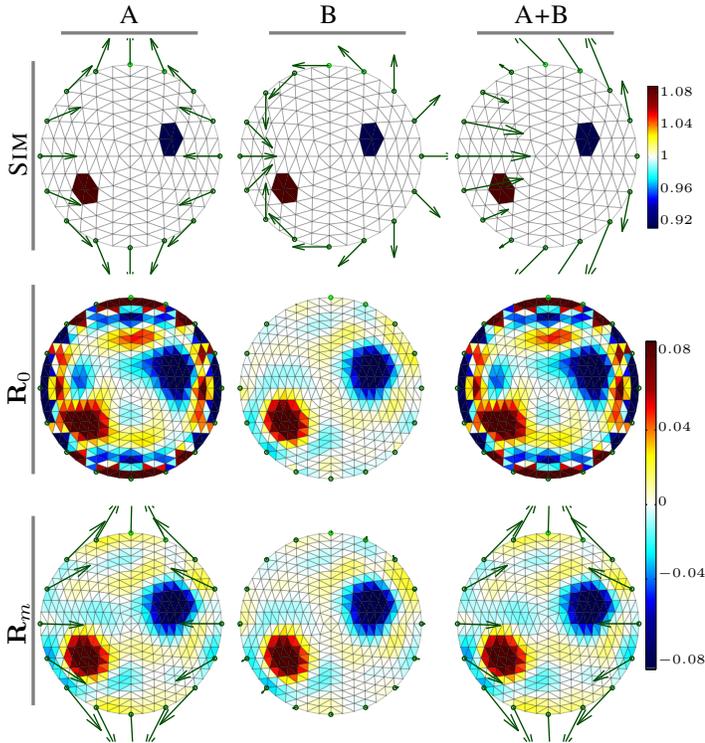
Fig. 8: Images reconstructed from three different movement patterns, illustrating that conformal distortion fields cannot be distinguished from conductivity changes. Green arrows indicate electrode movement ($40\times$ exaggeration).
A: Non-conformal distortion field $z \rightarrow 0.99x + \text{i}1.01y$.
B: Conformal distortion field $z \rightarrow z + 0.01z^2$.
A+B: Combined conformal and non-conformal distortion field.
SIM: Simulation movement and conductivity change pattern.
$\mathbf{R}_0$: Reconstruction assuming only conductivity change.
$\mathbf{R}_m$: Reconstruction of conductivity change and movement.

pan providing connectivity to the EIT system (Figure 9). The thickness of the gasket allowed the electrodes to be securely attached to the phantom as it was deformed.

A 16 electrode Goe-MF II EIT system (CareFusion, San Diego, USA) was used to take measurements from the deformable phantom. The ring was submerged in a saline bath where the bottom of the ring was in contact with the bottom of the container, and the top of the ring broke the surface to provide insulation between the saline solution inside and outside of the ring. The salinity was 0.68% (NaCl) which gave a nominal electrical impedance of 250Ω between adjacent electrodes.

Measurements were taken with the phantom in an approximately circular (relaxed) arrangement, with a side-to-side compression from two points, and with the ring under three points of compression (Figure 10). For each of these deformations, measurements were obtained where a circular conductive target was moved within the phantom.

The physical displacements of the electrodes were found by taking a digital photograph from above the phantom. A piece of graph paper was placed under the phantom and was taped to the bottom of the pan. The locations of the electrodes were

measured from the photograph and normalized using the graph paper grid.

The square root of the sum of squared errors (the 2-norm) in initial electrode location relative to a circular model of a radius matching the mean radius of the true electrode locations was found to be 0.0662mm. This indicated a fairly good match between the initial state of the phantom and the circular model in the reconstruction. The majority of the error norm was found to be related to errors in the angular location of the electrodes rather than the radial displacement. The mean of angular electrode error was found to be $1.3°$, where electrodes were expected every $22.5°$: a 5.8% mean angular error.

The estimated electrode displacements were found using the electrode perturbation algorithm as described earlier [9]. Boundaries were fitted to both the estimated and true electrode displacements using a Fourier series which allowed both rotation and radial displacements:

$$\theta' = \theta + \sum_{n=0}^{N} a_{\theta,n} \cos(n\theta) + b_{\theta,n} \sin(n\theta) \tag{39a}$$

$$r' = r \sum_{n=0}^{N} a_{r,n} \cos(n\theta) + b_{r,n} \sin(n\theta) \tag{39b}$$

With $N = 5$, reasonable fits to the displaced electrode locations were obtained. Using the fitted boundary, the norm of the error in the parameters was found (Figure 11, Figure 12).

For all cases except where no deformation occurred, it was found that the majority of the error was in the $a_{r,0}$ term which corresponds to a simple dilation.

These results are show in Table I, where a homogeneous undeformed first measurement $\mathbf{v}_{t1}$ was used as a reference against the second measurement $\mathbf{v}_{t2}$ taken under the deformation condition (Figure 10) and target type indicated in the table. The resulting error norm was calculated as described above for all 5 terms of (39a), (39b) and for only the first term. The last two rows of the table provide figures as representative examples of a conductive and insulating target under deformation (Figure 11 and Figure 12 respectively).
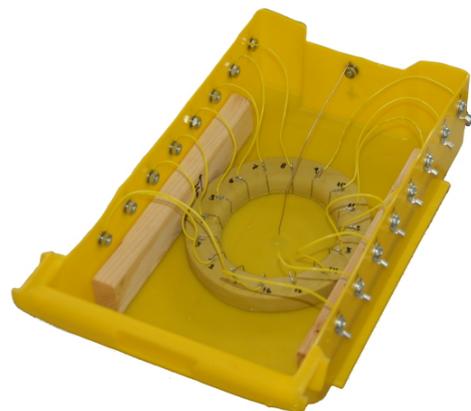

Fig. 9: Photograph of the phantom, built from a rubber gasket and stainless steel electrodes. The yellow dish is filled with a saline solution.

TABLE I: Boundary Reconstruction Accuracy

Deformation	Target	Parameter Errors		Comment
		All Errors	$a_{r,0}$ Errors *	
None	none	0.004	0.000	
	conductor	0.290	0.000	
	insulator	1.180	0.000	
2-point	none	0.296	0.156	
	conductor	0.706	0.503	
	insulator	1.241	0.674	
3-point	none	0.246	0.161	
	conductor	0.144	0.079	Figure 11
	insulator	0.336	0.241	Figure 12

* $a_{r,0}$ parameter from the Fourier series (39b)

V. Summary and Discussion

This work explores shape deformations and their effect on EIT measurements from three perspectives. A continuum model shows how conductivity can be modified to maintain the same boundary measurements through a shape deformation and furthermore, that only conformal shape deformations are possible when conductivity is restricted to isotropic values. This was tested in two ways: in simulations and with a deformable phantom. Results from simulations and the deformable phantom show that conformal deformations cannot be reconstructed from EIT measurements alone but do not affect reconstruction quality, while non-conformal deformations do cause significant artifacts but can be corrected to some degree by movement compensation algorithms such as that of Soleimani *et al.* [9].

We describe the mathematical constraints under which conformal deformations occur in EIT images. A conformal deformation is one in which angles are preserved (but not necessarily lengths) and thus, has some special behaviour in the context of EIT. A non-conformal deformation is one that is explicitly not conformal such that angles are not preserved. The results show that for any boundary deformation a corresponding conformal map can be found, and hence, any boundary deformation can be decomposed into its conformal and non-conformal components. For the interpretation of EIT images this means, while movement compensation such as that provided by the algorithm of Soleimani *et al.* can provide a strong benefit in reducing or removing significant artifacts, reduced artifacts do not lead to correctly located conductivity distributions without a correct boundary configuration. Recent studies have shown the importance of shape in locating the conductivity distribution correctly [24].
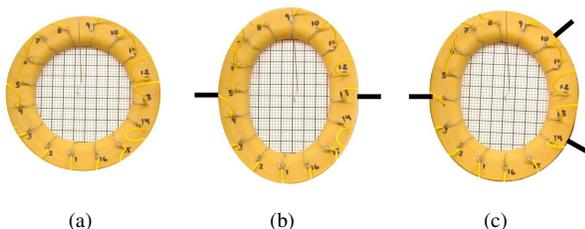
Fig. 10: Compressions: none (a), 2 points (b), 3 points (c)

(a) Displacements (b) $\mathbf{R}_0$ (c) $\mathbf{R}_m$
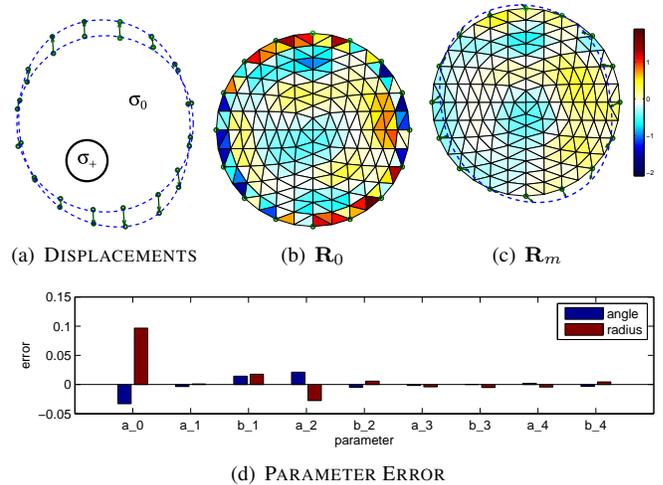
(d) Parameter Error

Fig. 11: Boundary reconstruction from electrode movement for 3-point compression with a conductive target; (a) the true displacements as measured from a digital photo with fitted boundary (dashed line), (b) a naïve reconstruction ($\hat{\mathbf{x}}_0 = \mathbf{R}_0 \mathbf{y}$) without the electrode perturbation algorithm; note the significant artifacts where the two images (b) and (c) are to the same colour scale, (c) the reconstructed electrode movement (green arrows) ($\hat{\mathbf{x}}_m = \mathbf{R}_m \mathbf{y}$) with fitted boundary (blue dashed line), (d) error in parameter values from fitted boundary between true and reconstructed images; parameters from (39a) (blue) (39b) (red)

Knowledge of this behaviour is useful when evaluating the performance of algorithms that correct for boundary movement because any boundary adaptive algorithm cannot detect the conformal component of the boundary movement if using electrical measurements alone and therefore, should not be penalized for their lack of performance on the conformal component of boundary movements. A conformal/non-conformal movement decomposition approach could be applied rather than the method used in the phantom experiments to take the true deformation of the phantom's boundary from the photographs and decompose it into its conformal and non-conformal components. The work here suggests that the conformal component should not match the reconstructed electrode movement while the non-conformal component should match up to a limit where the FEM mesh structure near the translated electrodes interferes with the free movement of those electrodes. This requires an implementation of the conformal/non-conformal decomposition which has not been achieved at this time.

In the convergence test, applying conformal deformations to the FEM mesh by translating nodes as described by the conformal vector field will not result in a locally conformal transformation because the actual shape of the element should bend to maintain the relative angle of the edges about each node. Convergence to machine precision is not achieved, but with a reduction in the size of elements, this inaccuracy was reduced and showed convergence towards an ideal conformally transformed mesh. Considering the effect of a conformal

deformation on a single element of the FEM mesh when using triangular two-dimensional linear expansion functions gives some insight into the behaviour of the entire FEM system under conformal deformations. The conformal deformations can be classified as translation, rotation, dilation, and inversion. These transformations are defined in infinitesimal terms while the FEM nodes exist as a discrete mesh. As a result, when the conformal transformation is applied to the FEM nodes, the element is not necessarily deformed in an exactly conformal manner. As the element size is reduced, the amount of discrepancy at a local level between an idealized deformation of the element, where its sides are bent, and the actual implementation, where the sides of the elements are always straight, approaches zero. This is not a new consideration. Treating a conformal map as a pair of conjugate discretely harmonic functions is deficient because the inverse of such a map, and the composition of two such maps, are no longer discretely conformal [25], [26].

This observation helps to explain why the convergence study presented here does not converge more rapidly. The convergence plot shows a trend toward convergence, but when the number of nodes is large, there is still a significant gap between the observed results (an error norm of 10^{-6}) and the hypothetical convergence towards machine precision (10^{-16}) that might be explained by the strictly triangular nature of the FEM elements. Using higher-order shape functions would not aid convergence unless the sides of the mesh elements were carefully aligned to the conformal deformation so that the angles at the corners of the elements were preserved. Isoparametric shape functions [27], [28] are capable of this type of shape distortion.

A linear reconstruction algorithm has been used in this work. A non-linear reconstruction algorithm would have only a small effect on the quality of the reconstructions because the problem has been selected to exhibit nearly linear behaviour through choosing small conductivity changes and small boundary movements. With larger conductivity changes a non-linear reconstruction algorithm may prove beneficial, but the boundary movement of algorithms such as that of Soleimani *et al.* are still restricted to small movements. The algorithm only moves the boundary nodes and therefore, is limited by the size of the mesh elements near that boundary.

In conclusion, this work illustrates the advantages and limits of reconstructing boundary shape for EIT. This work shows that selecting an appropriate boundary can significantly reduce the quantity of artifacts in a reconstructed image.

ACKNOWLEDGEMENTS

(a) DISPLACEMENTS (b) $\mathbf{R}_0$ (c) $\mathbf{R}_m$
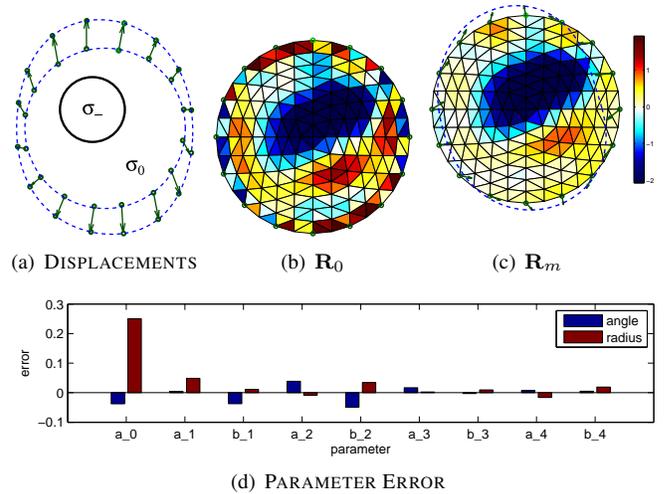
(d) PARAMETER ERROR

Fig. 12: Boundary reconstruction from electrode movement for 3-point compression with an insulating target; (a) the true displacements as measured from a digital photo with fitted boundary (dashed line), (b) a naïve reconstruction ($\hat{\mathbf{x}}_0 = \mathbf{R}_0\mathbf{y}$) without the electrode perturbation algorithm; note the significant artifacts where the two images (b) and (c) are to the same colour scale, (c) the reconstructed electrode movement (green arrows) ($\hat{\mathbf{x}}_m = \mathbf{R}_m\mathbf{y}$) with fitted boundary (blue dashed line), (d) error in parameter values from fitted boundary between true and reconstructed images; parameters from (39a) (blue) (39b) (red)

REFERENCES

[1] A. Adler, R. Guardo, and Y. Berthiaume, "Impedance imaging of lung ventilation: do we need to account for chest expansion?" *IEEE Trans. Biomed. Eng.*, vol. 43, no. 4, pp. 414–420, Apr. 1996.

[2] N. Coulombe, H. Gagnon, F. Marquis, Y. Skrobik, and R. Guardo, "A parametric model of the relationship between EIT and total lung volume," *Physiol. Meas.*, vol. 26, no. 4, pp. 401–411, Aug. 2005.

[3] W. R. B. Lionheart, "Boundary shape and electrical impedance tomography," *Inv. Prob.*, vol. 14, no. 1, pp. 139–147, Feb. 1998.

[4] M. Hazewinkel, Ed., *Encyclopaedia of Mathematics*. Springer-Verlag, 2002, ch. Conformal mapping.

[5] L. M. Heikkinena, M. Vauhkonena, T. Savolainena, K. Leinonenb, and J. Kaipioa, "Electrical process tomography with known internal structures and resistivities," *Inverse Problems in Engineering*, vol. 9, no. 5, pp. 431–454, 2001.

[6] A. Borsic, C. McLeod, W. Lionheart, and N. Kerrouche, "Realistic 2D human thorax modelling for EIT," *Physiol. Meas.*, vol. 22, no. 1, 2001.

[7] A. Tizzard, L. Horesh, R. Yerworth, D. Holder, and R. Bayford, "Generating accurate finite element meshes for the forward model of the human head in EIT," *Physiol. Meas.*, vol. 26, no. 2, 2005.

[8] S. Pulletz, A. Adler, M. Kott, G. Elke, B. Gawelczyk, D. Schädler, G. Zick, N. Weiler, and I. Frerichs, "Regional lung opening and closing pressures in patients with acute lung injury," *Journal of Critical Care*, 2011, in press.

[9] M. Soleimani, C. Gómez-Laberge, and A. Adler, "Imaging of conductivity changes and electrode movement in EIT," *Physiol. Meas.*, vol. 27, no. 5, pp. S103–S113, May 2006.

[10] V. Kolehmainen, M. Lassas, and P. Ola, "The Inverse Conductivity Problem with an Imperfectly Known Boundary," *SIAM J. Appl. Math.*, vol. 66, no. 2, pp. 365–383, 2005.

[11] ——, "Calderón's Inverse Problem with an Imperfectly Known Boundary and Reconstruction Up to a Conformal Deformation," *SIAM J. Math. Anal.*, vol. 42, no. 3, pp. 1371–1381, 2010.

[12] ——, "The Inverse Conductivity Problem with an Imperfectly Known Boundary in Three Dimensions," *SIAM J. Appl. Math.*, vol. 67, no. 5, pp. 1440–1452, 2007.

[13] ——, "Electrical Impedance Tomography Problem With Inaccurately Known Boundary and Contact Impedances," *IEEE Trans. Med. Imag.*, vol. 27, no. 10, pp. 1404–1414, 2008.

[14] A. Boyle and A. Adler, "Impact of electrode area, contact impedance and boundary shape on EIT images," *Physiol. Meas.*, vol. 32, no. 7, Jul. 2011.

[15] R. Kohn and M. Vogelius, "Identification of an unknown conductivity by

means of measurements at the boundary in Inverse Problems," in *AMS Proceedings*, D. McLauchlin, Ed., vol. 14. SIAM, 1984, pp. 113–123.

[16] ——, "Relaxation of a variational method for impedance computed tomography," *Communications on Pure and Applied Mathematics*, vol. 40, no. 6, pp. 745–777, Nov. 1987.

[17] R. Bishop and S. Goldberg, *Tensor Analysis on Manifolds*. Dover Publications, Inc., 1980.

[18] S. Goldberg, *Curvature and Homology*. Dover Publications, 1982.

[19] M. Schottenloher, *A Mathematical Introduction to Conformal Field Theory*. Springer, 2008.

[20] J. Marsden and M. Hoffman, *Basic Complex Analysis*. W.H. Freeman & Company, 1998.

[21] A. Adler and W. R. B. Lionheart, "Uses and abuses of EIDORS: An extensible software base for EIT," *Physiol. Meas.*, vol. 27, no. 5, pp. S25–S42, May 2006.

[22] A. Adler and R. Guardo, "Electrical impedance tomography: Regularised imaging and contrast detection," *IEEE Trans. Med. Imag.*, vol. 15, pp. 170–179, 1996.

[23] C. Gómez-Laberge and A. Adler, "Direct eit jacobian calculations for conductivity change and electrode movement," *Physiol. Meas.*, vol. 29, no. 6, pp. S89–S99, 2008.

[24] B. Grychtol, W. R. B. Lionheart, G. K. Wolf, M. Bodenstein, and A. Adler, "The importance of shape: thorax models for GREIT," in *Conf EIT 2011*, Bath, UK, May 2011.

[25] L. Kharevych, B. Springborn, and P. Schröder, "Discrete conformal mappings via circle patterns," *ACM Trans. Graphics*, vol. 25, no. 2, Apr. 2006.

[26] B. Springborn, P. Schröder, and U. Pinkall, "Conformal equivalence of triangle meshes," in *ACM SIGGRAPH ASIA*, 2008.

[27] I. Ergatoudis, B. Irons, and O. Zienkiewicz, "Curved, isoparametric, "quadrilateral" elements for finite element analysis," *Int. J. Solids Structures*, vol. 4, no. 1, pp. 31–42, Jan. 1968.

[28] M. Zlámal, "Curved elements in the finite element method," *SIAM J. Numer. Anal.*, vol. 10, no. 1, Mar. 1973.